



Multi-site harmonization of MRI data uncovers machine-learning discrimination capability in barely separable populations: An example from the ABIDE dataset

Sara Saponaro^{a,b}, Alessia Giuliano^c, Roberto Bellotti^{d,e}, Angela Lombardi^{d,e,*}, Sabina Tangaro^{e,f}, Piernicola Oliva^{g,h}, Sara Calderoni^{i,j}, Alessandra Retico^b

^a University of Pisa, Pisa, Italy

^b National Institute for Nuclear Physics (INFN), Pisa Division, Pisa, Italy

^c Medical Physics Department, San Luca Hospital, 55100 Lucca, Italy

^d Physics Department, University of Bari Aldo Moro, Bari, Italy

^e National Institute of Nuclear Physics (INFN), Bari Division, Bari, Italy

^f Department of Soil, Plant and Food Sciences (DISSPA), University of Bari Aldo Moro, Bari, Italy

^g Department of Chemistry and Pharmacy, University of Sassari, Sassari, Italy

^h National Institute for Nuclear Physics (INFN), Cagliari Division, Cagliari, Italy

ⁱ Developmental Psychiatry Unit – IRCCS Stella Maris Foundation, Pisa, Italy

^j Department of Clinical and Experimental Medicine, University of Pisa, Pisa, Italy

ARTICLE INFO

Keywords:

Harmonization
ASD
Machine learning
FreeSurfer
Multi-site

ABSTRACT

Machine Learning (ML) techniques have been widely used in Neuroimaging studies of Autism Spectrum Disorders (ASD) both to identify possible brain alterations related to this condition and to evaluate the predictive power of brain imaging modalities. The collection and public sharing of large imaging samples has favored an even greater diffusion of the use of ML-based analyses. However, multi-center data collections may suffer the batch effect, which, especially in case of Magnetic Resonance Imaging (MRI) studies, should be curated to avoid confounding effects for ML classifiers and masking biases. This is particularly important in the study of barely separable populations according to MRI data, such as subjects with ASD compared to controls with typical development (TD). Here, we show how the implementation of a harmonization protocol on brain structural features unlocks the case-control ML separation capability in the analysis of a multi-center MRI dataset. This effect is demonstrated on the ABIDE data collection, involving subjects encompassing a wide age range. After data harmonization, the overall ASD vs. TD discrimination capability by a Random Forest (RF) classifier improves from a very low performance ($AUC = 0.58 \pm 0.04$) to a still low, but reasonably significant $AUC = 0.67 \pm 0.03$. The performances of the RF classifier have been evaluated also in the age-specific subgroups of children, adolescents and adults, obtaining $AUC = 0.62 \pm 0.02$, $AUC = 0.65 \pm 0.03$ and $AUC = 0.69 \pm 0.06$, respectively. Specific and consistent patterns of anatomical differences related to the ASD condition have been identified for the three different age subgroups.

1. Introduction

Autism spectrum disorders (ASD) is a diagnostic category of neurodevelopmental disorders defined by persistent social communication and social interaction deficits, as well as restricted, repetitive patterns of behaviour, interests or activities that must be present in the early developmental period and cause clinically significant impairment in

social, occupational or other important areas of functioning (American Psychiatric Association et al., 2013). One of the key characteristics of autism is its great heterogeneity across multiple levels, including genetic background (Sullivan et al., 2012), neuroanatomical substrates (Pagnozzi et al., 2018), and phenotypic profile (Georgiades et al., 2013).

Despite the diagnosis of ASD is still made on the basis of direct behavioral evaluation of the child and parent/caregiver interview,

* Corresponding author.

E-mail address: angela.lombardi@uniba.it (A. Lombardi).

<https://doi.org/10.1016/j.nicl.2022.103082>

Received 20 January 2022; Received in revised form 6 June 2022; Accepted 6 June 2022

Available online 8 June 2022

2213-1582/© 2022 The Author(s). Published by Elsevier Inc. This is an open access article under the CC BY-NC-ND license (<http://creativecommons.org/licenses/by-nc-nd/4.0/>).

neuroimaging has been playing a fundamental role in identifying the neural correlates of this condition since the early 2000s (Courchesne et al., 2001).

In the last decade, machine learning (ML) techniques have been implemented in the attempt to discover neuroimaging-based biomarker of ASD, intended to either support, facilitate or shorten the diagnostic process (Ecker et al., 2015; Li et al., 2017). After the first encouraging results obtained for adults (Deshpande et al., 2013; Ecker, Marquand et al., 2010; Ecker, Rocha-Rego et al., 2010) and children with ASD (Calderoni et al., 2012; Gori et al., 2015; Ingalhalikar et al., 2011; Jiao et al., 2010; Uddin et al., 2013) on rather limited size datasets, the need of replicating the findings on larger samples emerged. However, inconsistent findings have been reported about the predictive power of ML techniques on neuroimaging data, and also regarding the possible patterns of alteration in the neuro-anatomy and in connectivity measures in ASD (Arbabshirani et al., 2017; Wolfers et al., 2019).

The aggregation of large data samples has been seen as a potential solution to overcome the fragmentation and lack of reproducibility of the previous studies. Large data samples are fundamental especially to conduct analyses based on ML techniques. Arbabshirani et al. (Arbabshirani et al., 2017) reported that the highest classification performances in case-control discrimination based on neuroimaging data are reached only in studies using small datasets. These performances drop significantly in larger samples, especially in multi-site databases. This observation holds also in the field of ASD research, where several large-scale studies (Abraham et al., 2017; Heinsfeld et al., 2018; Katuwal et al., 2016; Nielsen et al., 2013) reported classification accuracy quite lower than previous studies conducted on smaller samples.

In the field of ASD research, a large and public accessible resource of neuroimaging and phenotypic information has been collected within the Autism Brain Imaging Data Exchange (ABIDE) initiative¹. Two worldwide multi-site and large-scale collections have been released so far, ABIDE I (Di Martino et al., 2014) and ABIDE II (Di Martino et al., 2017), jointly consisting in more than a thousand cases and as many controls. In spite of the increased sample sizes, studies based on the ABIDE cohort continued to report highly variable classification performances (Vargason et al., 2020). In the work by Haar et al. (Haar et al., 2016) the modest accuracy in the case-control discrimination (<60%) suggested that anatomical measures are of limited diagnostic utility for ASD. It was highlighted afterwards that multi-center MRI data collections suffer from the so-called batch effect (Ferrari, Bosco et al., 2020; Ferrari, Retico et al., 2020; Lombardi et al., 2020). In brief, MRI data acquisitions made with different scanners and/or with different acquisition protocols encode confounding information in data which, if not accounted for, may completely mask case-control differences. In the specific case of ASD vs. control comparisons, the possible differences are so tiny that they can be completely obscured by the batch (or site) effect. In this context, Ferrari and colleagues observed that the acquisition site heavily confounds the ML classifiers, which instead need to be trained on a cleaned and controlled data sample. By adopting this method, i.e. limiting the ML training to a cohort of subjects acquired at one single site and controlling for all other confounding variables, the case-control discrimination performance of AUC = 0.79 was obtained on an independent test set (Ferrari, Bosco et al., 2020).

A data harmonization protocol devoted to the elimination of the site effect in neuroimaging studies has been introduced by Fortin et al. (Fortin et al., 2017), as an adaptation of the *ComBat* method developed by Johnson et al. (Johnson et al., 2007) to remove batch effects in genomics data. Pomponio et al. (Pomponio et al., 2020) have recently presented a modified version of the harmonization protocol, the *NeuroHarmonize* tool, which is suitable to harmonize pooled dataset in the presence of non-linear age trends. They developed and validated the methodology on a dataset of structural brain scans of more than 10

thousands subjects without known neurological or psychiatric disorders, covering the entire lifespan.

In this study, we evaluated the impact of the implementation of the *NeuroHarmonize* data harmonization protocol in the ASD vs. control discrimination problem tackled with ML. We implemented a standard Random Forest (RF) classifier to this purpose, and we analyzed the multi-center ABIDE I and ABIDE II data collections. First of all, we verified the successful removal of the site effect by the harmonization protocol. To this purpose, we first observed the confounding effect of the acquisition site on a ML classifier by evaluating non-null performances (AUC = 0.5) in the site vs. site discrimination by a RF trained on non-harmonized data of control subjects. Then, we observed the AUC values return to the expected range (AUC ~0.5) for the same classification problem after the harmonization process. Secondly, we quantified the increment in the two-class (i.e. ASD vs. control) RF classification performance after data harmonization. We evaluated this increment for both the whole sample and within each of three age-specific subgroups, namely children, adolescents and adults. Finally, for each age-specific subgroup, we identified the neuroanatomical features that contributed the most to the two-class separation. We thus highlighted specific patterns of brain feature involvement in the ASD condition across the lifespan.

2. Materials and methods

2.1. Participants and data description

We analyzed the structural MRI (T₁-weighted) brain scans of the ABIDE I (Di Martino et al., 2014) and ABIDE II (Di Martino et al., 2017) publicly available collections. The total dataset is composed by 2226 subjects (1060 subjects with ASD and 1166 controls with typical development (TD)), collected across 26 international institutions. The MRI scans belong to 39 different samples, which in this paper will be referred to as different sites, each of them containing images acquired with a particular scanner type and specific acquisition parameters. We performed the *recon-all* FreeSurfer preprocessing pipeline, which was unsuccessful for the images of poor quality. We performed manual quality control of these scans by visual inspection and we verified the presence of motion artifacts and of low signal to noise ratio. Hence, we discarded 65 subjects out of the 2226 scans available.

To allow the use of *NeuroHarmonize* tool, it is necessary that both data from case and control subjects are available within each site; thus, we had to exclude from the analysis two sites (KUL-II and NYU2-II of the ABIDE II cohort) that contributed to the collection exams of control subjects only. Since 97% of the subjects were under the age of 40 years, we limited our study to subjects aged 6 to 40 years only, similarly to other studies in the field (Haar et al., 2016; Katuwal et al., 2016). Moreover, we restricted our analysis to male subjects, due to the limited representation of female subjects in the ABIDE collection (<20% of subjects, spread over different sites and a wide age range). Due to the significant differences in neuroanatomy between males and females both in children (Retico et al., 2016) and in adults (Lai et al., 2013), we preferred to avoid including in this study the additional heterogeneity factor attributable to gender effects.

Thus, we obtained a final sample of N = 1638 subjects from 37 sites, including N = 845 typically developing participants with mean age = 15.6 years, standard deviation (STD) of age = 7.0 years and age range = [6.3- 40] years, and N = 793 subjects with ASD with mean age = 15.2 years, STD of age = 6.3 years and age range = [6.4- 40] years. A summary of the sample sizes of the ABIDE I and II cohorts included in this study and of the participants' average age is reported in Table 1. Fig. 1 shows a bar diagram reporting the number of subjects belonging to each site grouped by diagnosis, whereas Fig. 2 shows the age distribution within each site in terms of box plots. To allow the reproducibility of the analysis, the identification numbers (IDs) of the participants selected in the final sample are reported in Supplementary Materials.

¹ https://fcon_1000.projects.nitrc.org/indi/abide/.

Table 1

Number of subjects of the ABIDE I and II cohorts considered in this study. Only male subjects in the age range of [6–40] years (y) are considered. The number of participants are provided per site and per diagnostic group, together with the average age and standard deviation of each group. *Abbreviation:* STD - standard deviation.

Centers	N		Average age (y)		STD age (y)	
	ASD	TD	ASD	TD	ASD	TD
BNI_A	14	11	22.1	22.5	5.6	6.3
CALTECH	13	11	24.9	24.6	6.8	6.8
CMU	11	10	26.2	27.1	5.9	6.1
EMC_A	21	22	8.2	8.3	1.2	1.0
ETH_A	12	24	20.6	23.9	3.5	4.5
GU_A	38	27	11.0	10.8	1.5	1.6
IP_A	14	10	15.4	23.2	5.1	8.4
IU_A	15	15	22.2	24.3	5.3	5.5
KKI	18	24	10.1	10.3	1.4	1.3
KKI_A	40	99	10.5	10.4	1.5	1.3
LEUVEN_A	14	14	21.9	23.4	4.1	3.0
LEUVEN_B	12	15	13.9	14.6	1.4	1.6
MAX_MUN	15	26	20.5	23.3	9.5	7.8
NYU	68	79	14.0	16.0	6.5	6.2
NYU_A	43	28	9.7	9.1	4.6	1.9
OHSU	13	15	11.7	10.1	2.2	1.1
OHSU_A	30	27	12.1	10.3	2.1	1.7
OILH_B	16	20	21.4	24.2	3.9	3.9
OLIN	17	14	16.3	16.9	3.1	3.8
PITT	26	22	19.9	19.8	7.3	6.8
SBL	11	13	29.9	32.5	3.4	6.3
SDSU	13	15	14.9	14.5	1.7	1.5
SDSU_A	26	23	12.6	13.4	3.3	3.1
STANFORD	15	15	10.1	10.2	1.6	1.7
SU_B	18	19	11.0	11.1	1.2	1.3
TCDA	21	21	14.8	15.6	3.3	3.1
TRINITY	24	25	17.3	17.1	3.6	3.8
UCD_A	14	10	14.6	15.0	2.1	1.9
UCLA_A	34	28	13.3	12.3	2.4	2.2
UCLA_B	12	11	12.8	12.2	1.9	1.2
UCLA_3	13	11	12.1	9.9	2.1	2.2
UM_A	35	36	12.5	13.6	2.3	3.3
UM_B	12	20	14.7	16.9	1.5	4.0
USM	56	43	21.8	21.4	6.3	7.6
USM_A	15	13	17.5	23.9	7.0	8.6
U_MIA_A	9	11	10.5	9.5	2.0	2.0
YALE	20	20	12.7	12.3	3.1	2.8
Total	793	845	15.2	15.6	6.3	7.0

2.2. Image processing and feature extraction

The MRI scans selected from ABIDE I and ABIDE II cohorts have been processed with Freesurfer (Fischl, 2012) version 6.0 with the *recon-all* pipeline². This procedure includes cortical surface modeling, spherical coordinate transformation, non-linear curvature registration, automated volumetric segmentation and cortical reconstruction. Among the outputs generated by the Freesurfer processing pipeline, the following brain features have been selected: the global measures and the subcortical features available in the file *aseg.stats* and the cortical features available in the bilateral files *aparc.stats*. In this way, a total number of 221 brain morphometric features have been obtained.

These brain descriptive characteristics can be grouped into³:

- 9 global quantities: left (L) and right (R) mean thickness, L and R cortex volumes, L and R cerebral white matter volume, cerebrospinal fluid volume, total gray volumes and the volume of segmented brain without ventricles;
- 26 volumes of sub-cortical structures and corpus callosum;

- 186 measures, including the volume, the mean and standard deviation of the thickness of 62 structures (31 per hemisphere) from the Desikan–Killiany–Tourville Atlas (Klein & Tourville, 2012): 14 in the temporal lobe, 20 in the frontal lobe, 10 in the parietal lobe, 8 in the occipital lobe and 10 in the cingulate cortex.

2.3. Multi-center data harmonization procedure

In this study, we used the publicly available Python package *NeuroHarmonize*⁴, the state-of-the-art tool for multi-site neuroimaging analysis developed by Pomponio et al. (Pomponio et al., 2020), to reduce potential biases and non-biological variability induced by site and scanner effects. This approach combines the *ComBat* harmonization pipeline (Fortin et al., 2018; Fortin et al., 2017; Johnson et al., 2007), which removes unwanted sources of variability, such as site differences, while preserving variations due to other biologically-relevant covariates, with the generalized additive model (GAM) (Hastie & Tibshirani, 1986; Wood, 2017). The latter introduces a penalized nonlinear term to describe age effects in order to capture non-linearities in age-related volume differences in brain anatomy.

The application of the harmonization process to studies focused on case-control comparisons requires the availability of data from an appropriate control population. Indeed, the harmonization model parameters are calculated from the TD population, and then the harmonization transformation is applied to the group of patients. In fact, the assumption behind the *NeuroHarmonize* approach is that each sample measurement is drawn from the same reference distribution, although subjects in each sample may differ in age, sex, and intracranial volume (ICV). Patients with structural brain alterations could violate this assumption and, further, including them in the harmonization process would attenuate disease-related effects (Pomponio et al., 2020). Indeed, for small sample sizes, distinguishing between effects related to the heterogeneity of a disease and site effects might be infeasible. Thus, the use of a relatively more stable TD population to normalize data has been shown to improve the case-control discrimination performances (Fortin et al., 2017; Linn et al., 2016).

The objective of our analysis was to discard from the Freesurfer brain measures the confounding effect attributable to different acquisition sites, while preserving the biological variability of the brain features; thus, following the approach proposed in Pomponio et al. (Pomponio et al., 2020), we estimated the *NeuroHarmonize* model parameter on the entire cohort of control subjects, by specifying the age as a covariate whose effect is to be preserved during the harmonization process. Finally, we applied the estimated model on the entire sample of subjects with ASD and TD controls.

2.4. Binary classification with Random Forests

We implemented in this study RF binary classifiers to distinguish subjects belonging to two different cohorts. The RF classification method uses bagging of decision trees in order to reduce the variance of single trees, and thus improve the prediction accuracy (Breiman, 2001). The RF training process consists in training a number of decision trees on randomly selected data samples, getting a prediction from each tree, and then selecting the best solution by means of voting. Random Forests are considered a highly accurate and robust method because of the number of decision trees participating in the process. Moreover, they are less prone to overfitting problems (Breiman, 2001). The main reason is that they take the average of the predictions by all trees, thus reducing the possible biases.

The classification performances can be evaluated in terms of sensitivity (true-positive ratio) and specificity. The trade-off between the sensitivity and the false-positive ratio (which corresponds to one minus

² <https://surfer.nmr.mgh.harvard.edu/fswiki/recon-all>.

³ The extensive list of analyzed brain features can be found in the supplementary materials.

⁴ <https://github.com/rpomponio/neuroHarmonize>.

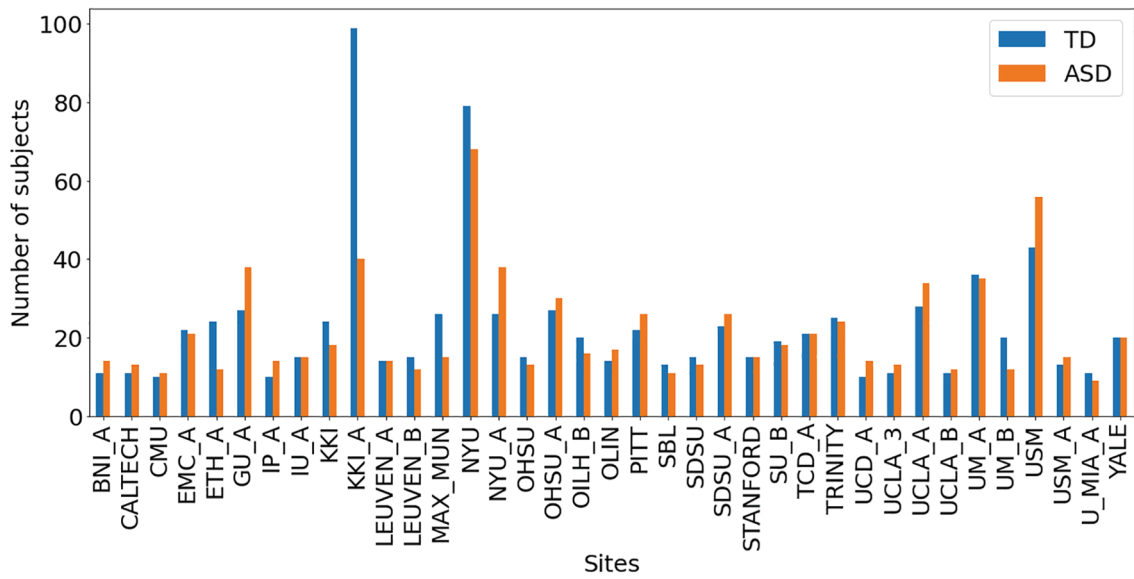


Fig. 1. Bar diagram showing the number of subjects acquired at each site for each diagnostic group.

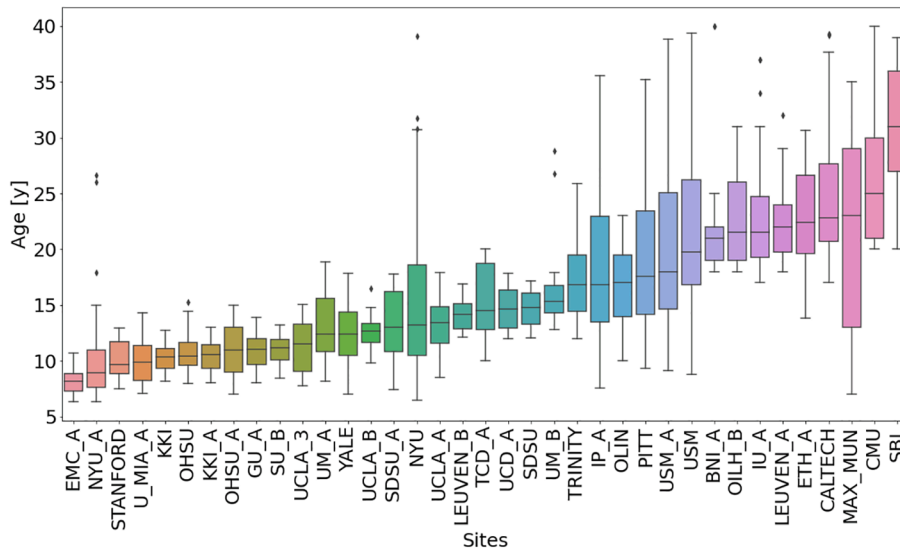


Fig. 2. Box plots showing the distribution of the age of the subjects belonging to each site, sorted by increasing median age.

the specificity), obtained by varying the decision threshold of the classifier, is known as the receiver operating characteristic (ROC) curve (Metz, 2006). From the ROC curve, the area under curve (AUC) can be estimated. The AUC is a global index to compare the ROC curves of different classifiers and represents the probability of correctly ranking a [case, control] pair (Hanley & McNeil, 1982).

We used the *RandomForestClassifier* in *Scikit-learn* (Pedregosa et al., 2011), a Python open-source machine learning library, and we set the number of trees to the default value of 500 and the number of candidate predictors considered at each split to $\sqrt{n_p}$, where n_p is the number of predictors (Breiman, 2001). The RF model has been trained according to a stratified 5-fold cross-validation scheme, which accounts for a comparable number of examples of the two classes in each subset to allow a balanced training. We implemented a feature scaling function (the *Scikit-learn RobustScaler*), that involves the subtraction of the median and the scaling with respect to the interquartile range (IQR). The IQR was computed within each fold of the 5-fold cross validation scheme. The AUC is computed within each fold; then, results across the 5 test folds

are used to calculate the mean and the standard deviation of AUC.

2.4.1. Assessment of the effectiveness of feature harmonization

A RF binary classification of control subjects from Site_i vs. Site_j (with $i \neq j$) has been carried out to evaluate whether and up to what extent the acquisition site is a confounding information for a ML classifier. A null discrimination ability (AUC ~ 0.5) is expected to be observed in case Site_i and Site_j are populated by control subjects with similar demographic characteristics, and in the absence of confounding site effects. In case $AUC \neq 0.5$ are detected, this could be ascribed either to differences in sample composition (e.g. in terms of age) or to confounding information encoded in the raw data during the acquisition. We expect that the data harmonization protocol is successful in removing the site effects, and this results in a reduced discrimination capability when attempting to predict site. Thus, in order to assess the effectiveness of the harmonization pipeline, we compared the Site_i vs. Site_j (with $i \neq j$) RF classification performances obtained before and after harmonization. The RF models have been trained in this case according

Table 2

Summary of the number of subjects (N) in each subgroup (Children, Adolescents and Adults). The mean and standard deviation (STD) of the age are reported in years (y) for each diagnostic group.

Subgroups	N		Mean age (y)		STD age (y)	
	ASD	TD	ASD	TD	ASD	TD
Children	301	345	9.8	9.9	1.5	1.3
Adolescents	352	309	15.3	15.2	2.3	2.4
Adults	140	191	26.2	26.5	5.2	5.1

to a stratified 50% hold-out validation scheme. The classification procedure was repeated 10 times, and the results were averaged to calculate the final value of AUC.

2.4.2. Evaluation of the impact of harmonization on case-control discrimination

Once the capability of the multi-center data harmonization process is demonstrated, the effect of this operation on the case-control discrimination ability of a RF classifier has been assessed. The RF classification of subjects with ASD vs. TDs has been carried out on both non-harmonized and harmonized data, in order to quantify the expected increment in the discrimination performance. To evaluate the significance of the classification performance achieved, we carried out a permutation test with 1000 repetitions. During the permutation testing the labels of the samples are changed randomly at each iteration and the classification task is repeated, thus simulating the null distribution of the performance metric under test, which is the AUC in our case. An empirical p-value is calculated as the percentage of times the score obtained is greater than the one obtained using the data with the original un-permuted class labels (Ojala & Garriga, 2009).

In addition to the analysis of the sample as a whole, we evaluated the RF classification performance across the lifespan, by partitioning the dataset into three subgroups by age: children ([6–12] years), adolescents ([12–20] years) and adults ([20–40] years), as summarized in Table 2. In subgrouping subjects by age, the thresholds were chosen because they approximately reflect pre-puberty, adolescence and early adulthood, and also because they allow to generate subgroups with a consistent and comparable number of subjects in each group (Katuwal et al., 2016).

It is worth specifying that the impact of the harmonization protocol in the whole sample and in the three age-specific subgroups is evaluated as follows: the harmonization protocol is applied on the whole sample (the harmonization model parameters are evaluated on the TD population and then the model is applied to the whole sample); then, RF classifiers are trained to distinguish ASD from TD subjects both on the non-harmonized and harmonized data in order to compare the performances. The latter operation is carried out for the whole sample and in the three age-specific subgroups.

2.5. Feature importance

Random Forest classifiers have the relevant advantage of allowing an embedded interpretable feature importance analysis (Chen & Ishwaran, 2012). Indeed, several techniques can be used to identify the particular set of features with relevant role in the classification process. We calculated the importance of each feature by using the *permutation importance* function implemented in *Scikit-learn*. The permutation feature importance is defined as the decrease in a model score when a single feature value is randomly shuffled. This procedure breaks the relationship between the feature and the target, thus the drop in the model score is indicative of how much the model depends on that feature. It can be summarized as follows:

- Take as input the fitted predictive model m on training dataset D
- Compute the accuracy score (s) of the model m on data D
- For each feature j :

- For each repetition k in $1, \dots, K$:
- * Randomly shuffle column j of data-set D to generate a corrupted version of the data named $D_{k,j}$.
- * Compute the score $s_{k,j}$ of model m on corrupted data $D_{k,j}$.
- Compute importance i_j for feature f_j defined as:

$$i_j = s - \frac{1}{K} \sum_{k=1}^K s_{k,j} \quad (1)$$

For the age-specific subgroups in the case of harmonized image features, we randomly mixed each feature 100 times, thus we obtained a sample of importance scores. Since a feature selection algorithm may be sensitive to changes in the training set, the feature importance was calculated as an average of the importance scores from 10 train folds. As the most important features, we selected the scores above the 90th percentile.

The effect size of ASD vs. TD group difference was quantified using Cohen's d coefficient. It consists in the standardized difference between two mean values μ defined as $(\mu_{ASD} - \mu_{TD}) / SD_{pooled}$, where SD_{pooled} is the weighted average of the standard deviations of the two groups (Cohen, 1988).

3. Results

3.1. Implementation and test of the data harmonization effectiveness

We estimated the harmonization model provided by the *Neuro-Harmonize* package on the control group consisting of 845 subjects, thus obtaining both the model parameters and the harmonized features for the control group. Then, we applied the model on the group of 793 subjects with ASD to obtain the dataset for the case-control comparison entirely harmonized for site effects. In this process, we used the site information as a model covariate and we specified the age parameter as a nonlinear term to be accounted for in the harmonization process in order to preserve the age trend of the brain descriptive features.

Fig. 3 shows how the harmonization procedure acts on the values of an example feature (the mean cortical thickness of the left hemisphere). It can be noticed that appreciable inter-site biases.

in the feature values are removed, whereas the expected age trend of the feature is preserved (in the case of the cortical thickness, a thinning with age occurs in normal neurodevelopment).

The effectiveness of the harmonization process in removing site-related biases has been quantified in terms of a measurable reduction of the confounding effect that site has on a RF binary classification. Fig. 4 shows the heatmaps of the AUC values obtained on non-harmonized and on harmonized data in the attempt to discriminate TD subjects acquired at Site $_i$ from those acquired at Site $_j$ with a RF classifier, according to ten repetitions of a stratified 50% hold-out validation scheme. As visible in panel (a) of the figure, extremely high AUC values are obtained in the site-by-site discrimination, based on non-harmonized features. Once the features have been harmonized, as shown in panel (b), the Site $_i$ vs. Site $_j$ discrimination capability of a RF classifier decreases to values closer to AUC 0.5, which is the expected null classification performance for indistinguishable cohorts. As visible in the bottom left corner of the map reported in panel (b), when comparing sites populated by TD subjects in different age ranges, the RF classifier maintains extremely high discrimination ability, as expected. Ultimately, the visual comparison between panel (a) and (b) of Fig. 4 highlights that the data harmonization process allows to recover homogeneity of sample features, thus AUC 0.5, in the Site $_i$ vs. Site $_j$ discrimination for pairs of sites in similar age ranges, i.e. site combinations reported close to the diagonal of the heatmaps.

3.2. ASD vs. TD discrimination performance

Random Forest classifier have been trained to distinguish subjects

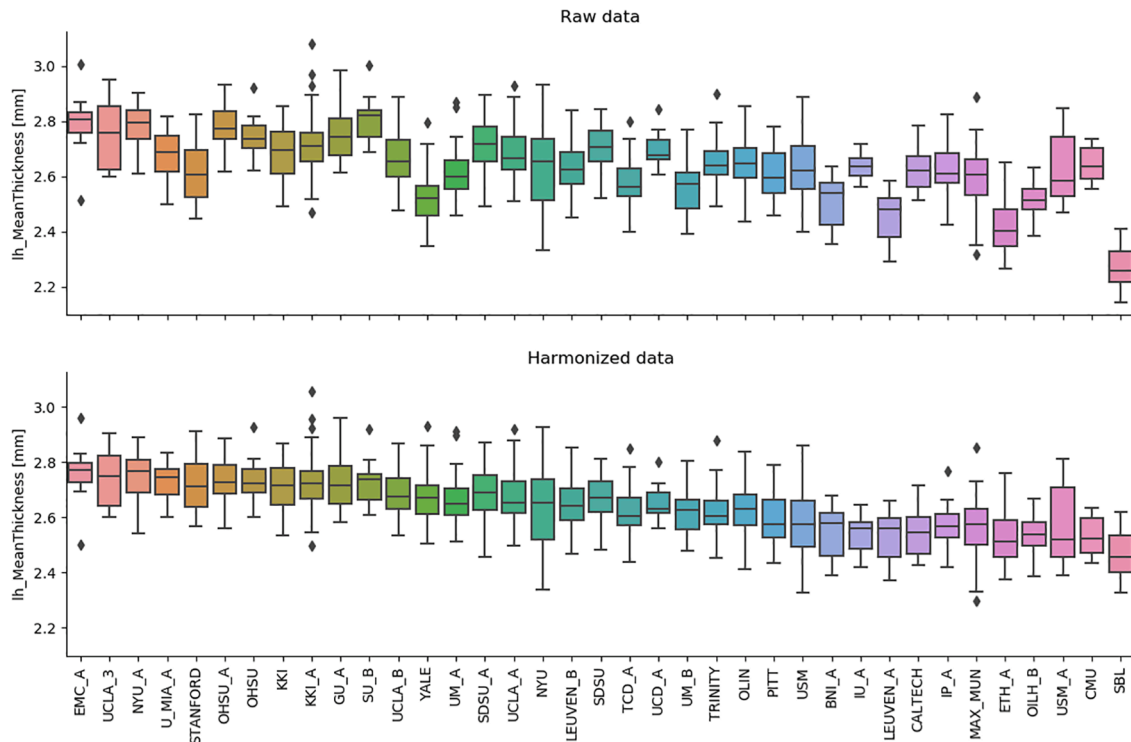


Fig. 3. The effect of the harmonization process on an example feature, the left hemisphere cortical thickness, is shown. The box plots show of the distributions of the features, grouped by site, the list of which is ordered by increasing median age. The presence of inter-site biases which is visible on raw data (top panel) is canceled by the harmonization process while preserving the expected age trend of the feature (bottom).

with ASD from TD controls on the whole sample and in the three age-specific subgroups, according to a 5-fold cross-validation scheme. The classification was performed both on the non-harmonized and on the harmonized datasets in order to evaluate the impact of the harmonization on the problem of ASD vs. TD categorization. Fig. 5 shows the ROC curves obtained on the whole sample by averaging the ROC curves computed on each of the 5 folds of the cross validation. The mean AUC values and the standard deviations are reported. An AUC of 0.58 ± 0.04 was achieved on non-harmonized data and an AUC of 0.67 ± 0.03 on harmonized data.

The performance in the ASD vs. TD discrimination by RF classifiers trained according to a 5-fold cross validation scheme, are reported in terms of the AUC, accuracy, sensitivity and specificity for the whole sample and in the three age-specific subgroups in Table 3. Both the results obtained on non-harmonized and on harmonized data are provided.

It is apparent from the results reported in the table that for the groups of children and adolescents the AUC values obtained on non-harmonized data are consistent with the chance level. To assign a statistical significance to the null hypothesis that the ASD and TD cohorts cannot be distinguished by a RF classifier, we carried out the permutation tests, whose results are shown in Fig. 6. The histograms of the AUC scores obtained at each permutation are reported in the figure. For each histogram, the red line indicates the score obtained by the RF classifier on data with the original un-permuted class labels. The empirical p values are thus computed for each AUC classification performance reported in Table 3, showing that in all cases, except for the classification of non-harmonized data of children and adolescents, as mentioned above, significant p values have been obtained.

3.3. Relevant brain features in the ASD vs. TD discrimination problem

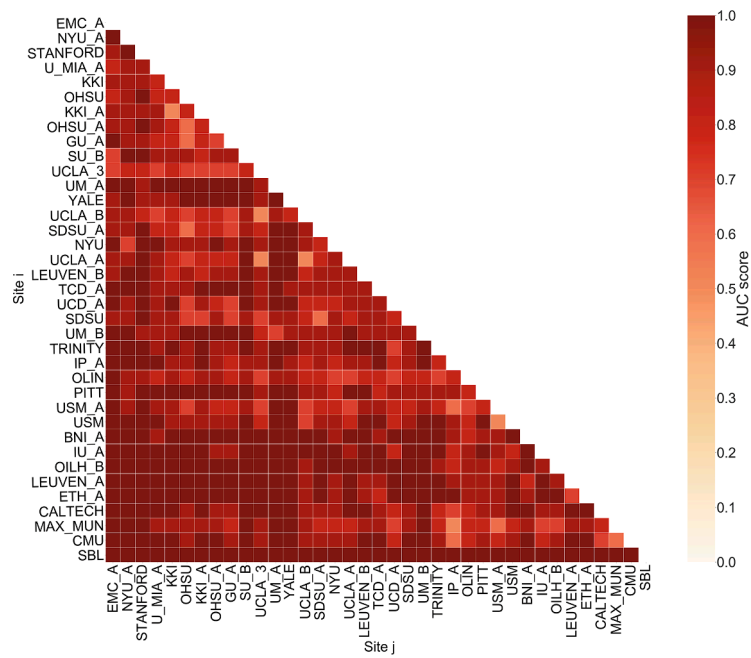
The most important features in the ASD vs. TD discrimination problem have been identified for the three age-specific subgroups by

exploiting the *permutation importance* function of *Scikit-learn*. The features whose importance scores exceeded the 90th percentile are reported in Table 4. In addition to the specification of the feature type (e.g. thickness or volume, average or standard deviation), the table reports the sign of the Cohen's d , thus indicating whether a feature mean is larger/smaller (+/-) in the sample of subjects with ASD with respect to TD controls.

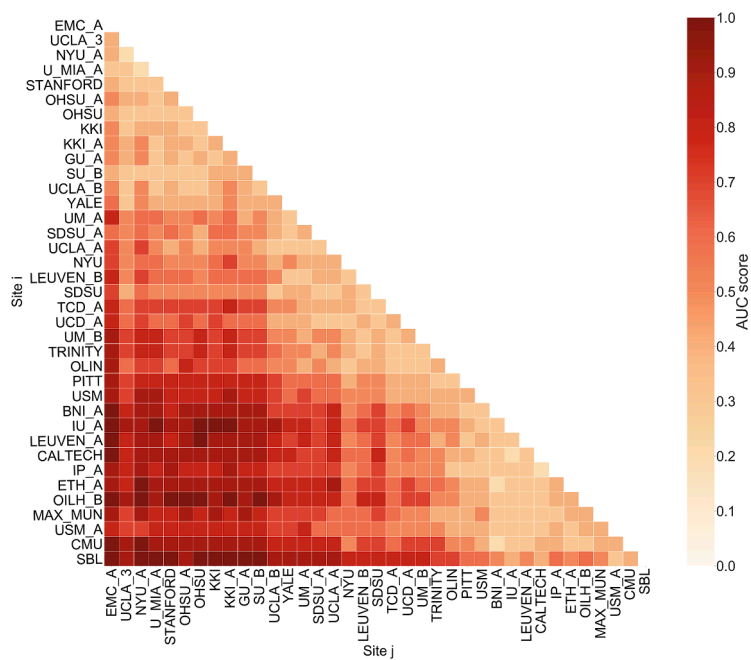
A visual representation of the relevant features is shown in Fig. 7, which allows an immediate identification of the set of features common to the different age-specific subgroups. It can be noticed from the table and the figure that the features identified as important in the ASD vs. TD discrimination problem were mainly from the frontal, parietal and temporal regions.

4. Discussion

We showed in this paper that the data harmonization is a necessary preprocessing step in the analysis of brain descriptive features extracted by MRI scans in multi-center studies. Several works demonstrated better performance after harmonization approaches. Qin et al. (Qin et al., 2022) applied ComBat on whole-brain functional networks to identify individuals with major depressive disorder from controls outperforming the accuracy values of other state-of-the-art methods. Wang et al. (Wang et al., 2022) developed a novel deep-learning domain adaptation framework to tackle the confounding effects for both Alzheimer's disease and Schizophrenia classification tasks by using the whole minimally preprocessed 3D T1-weighted brain MRI scans of the subjects. Monte-Rubio et al. (C. Monte-Rubio et al., 2022) proposed an approach using the predictive probabilities provided by Gaussian processes to harmonize multi-site T1-weighted MRI data for Parkinson's disease classification. Although the latter two methodologies cannot be applied to data extracted from preprocessed images such as cortical and subcortical features, the authors highlighted that harmonization is a crucial preprocessing step to be performed before any clinical



(a) Heatmap obtained on non-harmonized data.



(b) Heatmap obtained on harmonized data.

Fig. 4. AUC values obtained in the RF classification of non-harmonized (a) and on harmonized (b) features of control subjects of Site_i vs. Site_j, according to a 5-fold cross validation protocol. The site list is sorted according to increasing median age of subjects at each site (see Fig. 2).

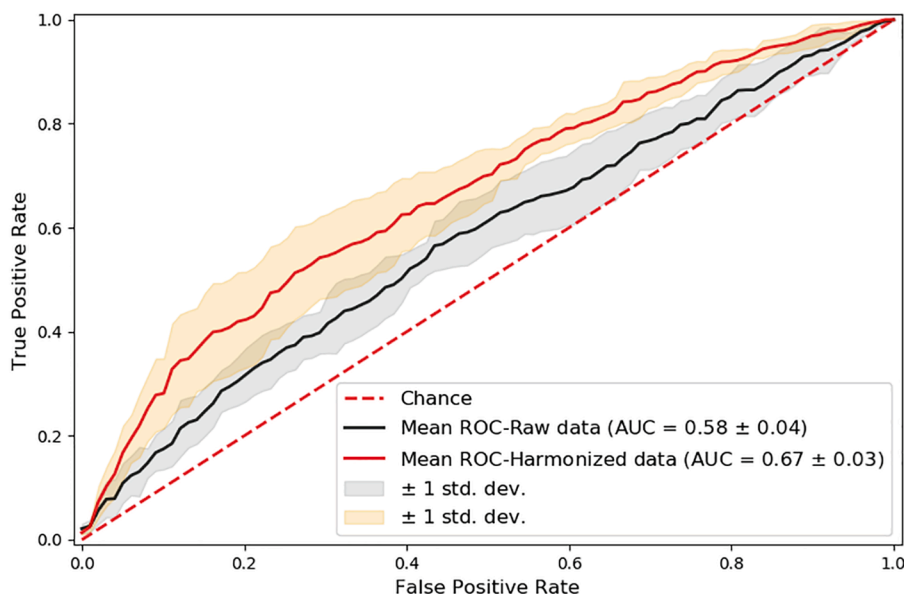


Fig. 5. ROC curves obtained for the ASD vs. TD classification within 5-fold cross-validation scheme on the whole dataset.

Table 3

Classification performances (AUC, accuracy, sensitivity and specificity) obtained in the ASD vs. TD discrimination by a RF classifier for the whole sample and in the subgroups of children, adolescents and adults on non-harmonized and on harmonized data. The average value and the standard deviation of each metric are computed according to a 5-fold cross validation scheme.

Sample	Data	AUC	Accuracy	Sensitivity	Specificity
Whole	Raw	0.58 ± 0.04	0.56 ± 0.02	0.54 ± 0.04	0.58 ± 0.02
	Harm	0.67 ± 0.03	0.62 ± 0.03	0.61 ± 0.06	0.63 ± 0.07
Children	Raw	0.52 ± 0.09	0.53 ± 0.05	0.68 ± 0.15	0.40 ± 0.21
	Harm	0.62 ± 0.02	0.59 ± 0.03	0.58 ± 0.05	0.60 ± 0.04
Adolescents	Raw	0.47 ± 0.07	0.49 ± 0.03	0.52 ± 0.25	0.46 ± 0.24
	Harm	0.65 ± 0.03	0.61 ± 0.01	0.59 ± 0.04	0.62 ± 0.03
Adults	Raw	0.62 ± 0.07	0.58 ± 0.04	0.54 ± 0.10	0.60 ± 0.06
	Harm	0.69 ± 0.06	0.68 ± 0.06	0.65 ± 0.07	0.70 ± 0.08

classification task. Our work addresses the problem of ASD vs. TD classification task. Our work focuses on the problem of the ASD vs. TD classification task, whose performance significantly improved after the harmonization procedure. The slightly over the chance-level AUC values obtained without any harmonization indicating the small differences between the two populations were obscured by confounding effects, reached the $AUC = 0.67 \pm 0.03$ after harmonization.

4.1. Comparison with the categorization performances reported in previous studies

Controversial results were reported by other studies regarding the ASD vs. TD discrimination performances of ML classifiers (Arbabshirani et al., 2017; Wolfers et al., 2019). In general, not fully replicated and lower results were reported, thus suggesting that the two groups are not highly separable. Limiting the comparison to previous ML analyses of structural MRI data of large cohorts of subjects such as the ABIDE I and ABIDE II collections, a historical overview is reported below to highlight

the evolution of the methodological approaches to the problem:

- the work by Haar et al. (Haar et al., 2016), analyzed a sample restricted to 590 subjects of the ABIDE I collection and then a sample relaxed to 906 subjects, reporting a modest accuracy in the case-control discrimination (<60%). This result is consistent with the almost-chance-level result that we obtained on non-harmonized data;
- in the work by Katuwal et al. (Katuwal et al., 2016) the low accuracy obtained in the study by Haar et al. (Haar et al., 2016) is attributed to the ASD heterogeneity. The authors applied ML classifiers to a group of 734 males (361 ASD vs. 373 TD of the ABIDE I collection), obtaining AUC values in the 61–68% range. Then, they repeated the analysis on more homogeneous subgroups in terms of age, intellectual quotient and autism severity and they obtained very high discrimination performance (AUC greater than 0.8) in specific subgroups. However, they did not take into account possible biases introduced by the site effect;
- the works by Ferrari et al. (Ferrari, Bosco et al., 2020; Ferrari, Retico et al. 2020) highlighted that the ABIDE I and ABIDE II multi-center data collections suffer from the so-called batch effect; thus, training the ML model on a subgroup of 86 subjects selected from the most populated site of the ABIDE collection, the NYU₁ dataset, an $AUC = 0.79$ on an independent test set (including subjects under 30 years of age and fully matched on demographic and clinical variables with the subjects of the training set) was obtained in the ASD vs. TD

discrimination problem; despite a trend in the ASD vs. TD discrimination capability of the classification pattern trained on the NYU₁ sample was shown in testing it on the whole ABIDE sample, significant classification performances were not achieved in that case, probably due to different demographic composition across centers and to site effects;

- the work by Gao et al. (Gao et al., 2021) implemented a deep convolutional neural network to carry out the ASD vs. TD classification based on the analysis of morphological covariance networks derived by structural MRI scans of a sample of 518 subjects with ASD and 567 TD controls of the ABIDE I collection; no harmonization strategy was implemented in that study, probably since the covariance networks are less sensitive to systematic site effects, and a classification accuracy of 71.8% was achieved. This result, despite provided without

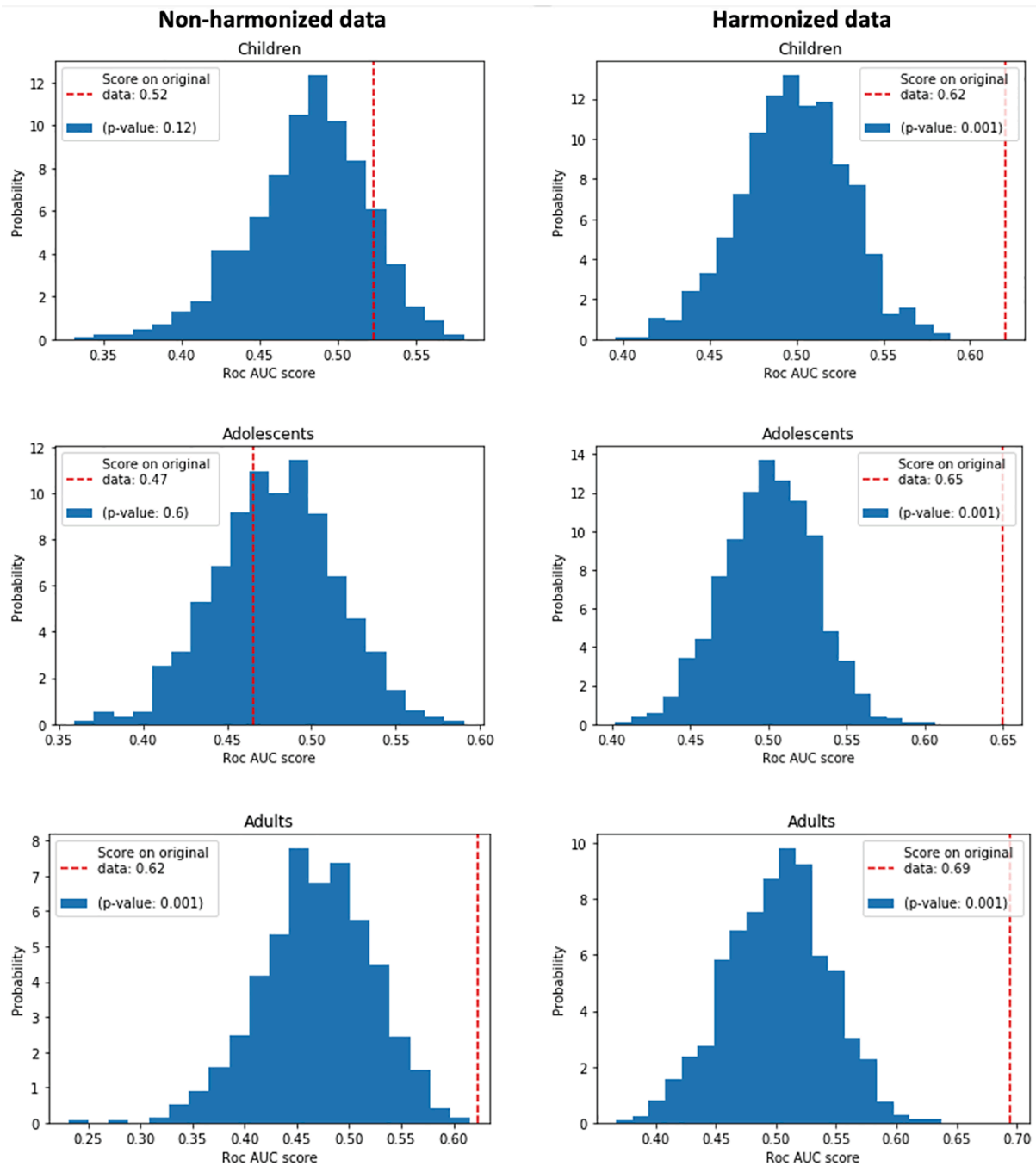


Fig. 6. Histograms reporting the AUC values obtained in the permutation test (with 1000 permutations) for the non-harmonized (left column) and the harmonized data (right column) of subjects belonging to groups of children, adolescents and adults. The vertical dashed red lines indicate the scores obtained by the RF classifiers on data with the original un-permuted class labels. (For interpretation of the references to colour in this figure legend, the reader is referred to the web version of this article.)

an estimate of the variability across the 10-fold cross validation implemented by the authors, slightly outperforms the best accuracy values we obtained. This may be due to the superior classification ability of deep learning classifiers compared to traditional ones.

As a general consideration regarding the modest classification performances achieved in our work, it is worth specifying that the aim of this study was to investigate the impact of a data harmonization strategy in a challenging classification problem. Thus, the systematic search for the best performing classifier was not within the objectives of this work. As an example, deep learning models could certainly lead to superior

discrimination performances if a sufficiently large dataset, adequately representing the heterogeneity of the population, is available to properly train them (Avanzo et al., 2021).

4.2. Methodological limitations of this study

A limitation of both the *ComBat* and *NeuroHarmonize* tools for multi-site data harmonization consists by the fact that these methods are particularly suitable to harmonize brain descriptive features (e.g. neuroanatomical (Fortin et al., 2018; Pomponio et al., 2020), connectivity (Ingahlhalikar et al., 2021) and diffusivity measures (Fortin et al.,

Table 4

The most important features (importance scores over the 90th percentile) in the RF classification for the three age-specific sub-groups are reported. The reported sign indicates whether the feature mean is larger/smaller (+/−) in the group of subjects with ASD with respect to TD controls.

Hemisphere	Anatomical region	Measurement		
		Children	Adolescents	Adults
lh	Caudal anterior cingulate		GrayVol(+)	GrayVol(+)
rh	Caudal anterior cingulate			ThickAvg(+)
lh	Entorhinal		ThickStd(+)	
rh	Entorhinal	ThickAvg(−)		
lh	Fusiform	ThickStd(+)	ThickAvg(+)	
rh	Fusiform		ThickStd(+)	
lh	Inferior parietal	GrayVol(−)		
rh	Inferior parietal	GrayVol(−)	ThickStd(+)	
lh	Inferior temporal	ThickStd(+)	ThickStd(+)	
rh	Inferior temporal	ThickAvg(−)		
lh	Isthmus cingulate	ThickStd(+)		
rh	Isthmus cingulate		GrayVol(+)	
lh	Lateral occipital	ThickAvg(+)	ThickAvg(+)	GrayVol(+)
lh	Lateral orbitofrontal		ThickAvg(+)	
rh	Lateral orbitofrontal		GrayVol(−)	
lh	Lingual		ThickStd(+)	ThickStd(+)
rh	Lingual	ThickAvg(+)	ThickAvg(+)	
lh	Medial orbitofrontal		ThickAvg(+), GrayVol(+)	ThickAvg(+)
rh	Medial orbitofrontal		ThickStd(+)	ThickAvg(+)
rh	Middle temporal	ThickAvg(−), ThickStd(+)		
lh	Paracentral			GrayVol(+), ThickStd(+)
rh	Paracentral	ThickAvg(−)		
rh	Parahippocampal			ThickAvg(−)
lh	Pars orbitalis	GrayVol(+)		
rh	Pars orbitalis			GrayVol(+)
rh	Pars triangularis	ThickStd(+)		
lh	Pericalcarine		ThickAvg(+)	
rh	Pericalcarine	GrayVol(−)		
lh	Posterior cingulate			ThickStd(+)
rh	Posterior cingulate	ThickAvg(+)		
rh	Precentral	ThickAvg(−)		
lh	Precuneus		ThickStd(+)	
rh	Precuneus		ThickStd(+)	
rh	Rostral anterior cingulate			ThickStd(+)
lh	Rostral anterior cingulate	GrayVol(+)		
lh	Superior frontal			GrayVol(+)
rh	Superior frontal			GrayVol(+)
rh	Superior temporal	ThickStd(+)	ThickAvg(+), ThickStd(+)	
lh	Supramarginal		ThickStd(+)	
rh	Supramarginal			GrayVol(+)
lh	Transverse temporal pole		ThickAvg(+)	GrayVol(+), ThickAvg(+)
	Central corpus callosum	Volume(−)		
	Middle anterior corpus callosum	Volume(−)		
lh	Amygdala			Volume(+)
rh	Caudate	Volume(+)		
rh	Hippocampus			Volume(+)
lh	Nucleus Accumbens		Volume(+)	
rh	Nucleus Accumbens	Volume(+)		
lh	Pallidum			Volume(+)
rh	Putamen			Volume(+)
lh	Thalamus			Volume(+)
rh	Ventral diencephalon			Volume(+)

2017)), whereas they are not directly applicable to process original MRI images. An approach devoted to the direct harmonization of the images acquired at different scanners has been proposed by Wrobel et al. (Wrobel et al., 2020). They implemented and evaluated according to a cross-validation scheme a multi-site image harmonization method based on the alignment of the intensity distributions of images acquired at different sites. Alternatively, the domain adaptation approach could be applied in order to avoid the need of harmonizing multi-center data before ML techniques are applied for data analysis and classification. This ML approach allows to handle the differences in data distributions between test and train domains and has been successfully applied to

analyse several functional connectivity measures derived from the multi-center ABIDE dataset (Bhaumik et al., 2018). Moreover, a deep-learning based implementation of the domain adaptation concept to analyze structural MRI scans has been implemented by Guan et al. (Guan et al., 2021) to eliminate the confounding site effect in a study of the Alzheimer's Disease.

The relevant features for the discrimination problem have been identified in our study in order to evaluate their consistency between the different age-specific subgroups and across the entire lifespan. An important issue of our work concerns the feature selection strategy: although a RF classifier can handle multicollinearity among features, it

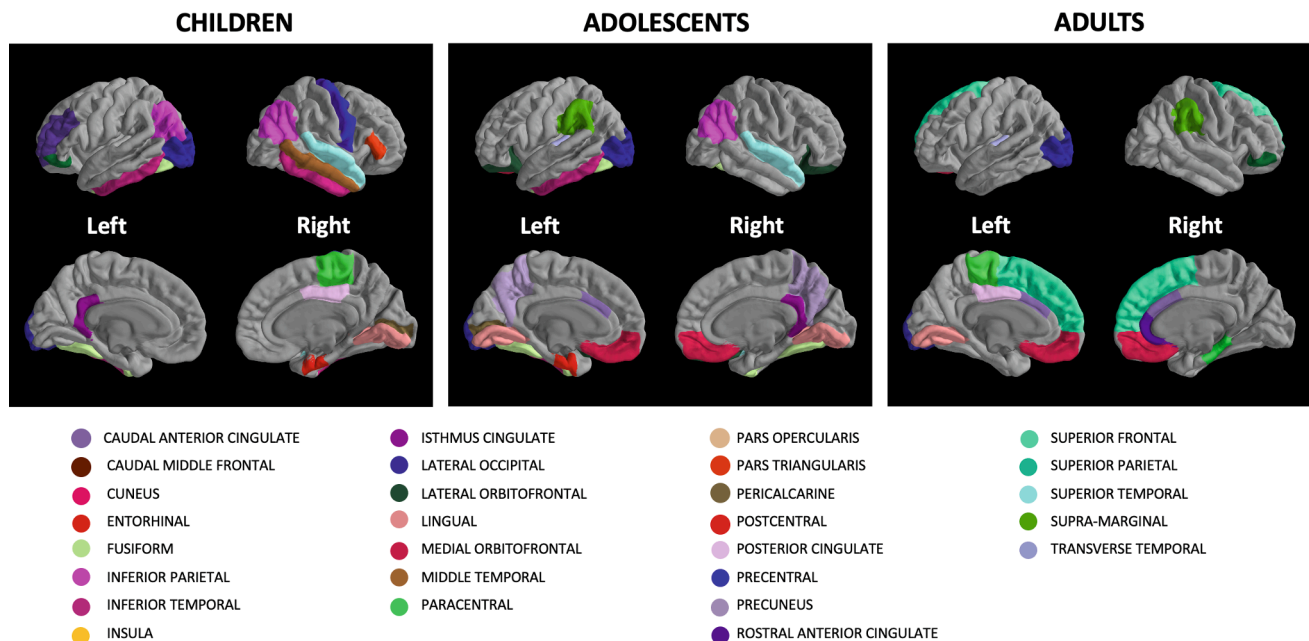


Fig. 7. The brain regions whose features were identified as relevant (see table 4) in the ASD vs. TD discrimination are highlighted on the MRI scan of the Freesurfer average sample subject. The PySurfer library has been used to produce this figure.

may not return all features with the same information content, yielding a minimal set of relevant features to optimize prediction and complicating the biological interpretation of the results. Although we applied the permutation feature importance method to mitigate this problem, further analysis would be required to completely overcome this issue and obtain the set of all regions relevant to discrimination.

4.3. Considerations of age-related class separability and relevance of important features

Despite the discrimination power of a RF classifier found in our study between the two classes of subjects with ASD and TD controls is moderate, the statistical significance of the separation capability has been demonstrated for the whole cohort and for the three age-specific subgroups. When the sample was divided by age group in children, adolescents and adults, we observed the highest discrimination ability of the RF classifier in adults, meaning that the brains of adults with ASD differ from the brains of age-matched controls more than the brains of children/adolescents with ASD differ from those of their peers. Relatively little is known about the factors that shape age-related brain changes in ASD: it is possible that the greater burden of brain alterations in adulthood could be traced back to the frequent association of ASD with other psychiatric disorders, mainly evident with increasing age. Indeed, according to a recent systematic review and meta-analysis (M.-C. Lai et al., 2019), ASD heighten the risk of developing major psychiatric disorders, and some of these (i.e. depressive, bipolar, and schizophrenia spectrum disorders) become more prevalent with increased age. Thus, the brain MRI alterations in adults with ASD could be the result not only of the ASD brain signature, but also of other comorbid psychiatric disorders, which contribute to making the underlying neural alterations greater. Crucially, the cross-sectional design of this investigation did not allow understanding the age-associated trajectory of brain alterations in the same subjects with ASD and longitudinal inferences about development from cross-sectional studies can be seriously misleading (Kraemer et al., 2000): therefore, ad-hoc longitudinal MRI studies in large and well-characterized ASD individuals are needed to answer this research question. Regarding the relevant brain structural features we identified in the ASD vs. TD binary classification with RF, we found out that only one region was consistently found among the most discriminant ones

across the whole lifespan: the lateral occipital gyrus of the left (L) hemisphere. Either the volume or the average thickness of this feature were found to be greater in the population of subjects with ASD with respect to controls. This brain region has been previously implicated in the pathogenesis of ASD, although with a decreased value in individuals with ASD compared to TD peers. Indeed, a recent investigation that combined multiple imaging modalities (structural MRI, DTI, and resting state fMRI) to investigate respectively brain anatomy, connectivity and function in a sample of forty boys with ASD detected that individuals with ASD have significantly reduced gray matter surface area, structural connectivity, and resting state brain activity in the lateral occipital cortex (Jung et al., 2019). Additionally, decreases in surface area, structural connectivity, and resting-state brain activity in this region were correlated with increased social symptom severity in subjects with ASD.

In addition, we observed age-specific cortical abnormalities. In this light, a number of consistently altered features between the groups of children and adolescents have been identified. Most of them (if not explicitly differently stated) showed increased values in subjects with ASD with respect to TD controls: the average thickness of the L fusiform gyrus and its standard deviation (SD); the thickness SD of the L inferior temporal gyrus; the volume (decreased in children with ASD) of the right (R) inferior parietal lobule (IPL) and its thickness SD (increased in adolescents with ASD); the average thickness of the R lingual gyrus; the average thickness and its SD of the R superior temporal gyrus. The increased cortical thickness of some brain regions in children and adolescents with ASD is consistent with data reporting an early brain overgrowth in ASD subjects. Both head circumference investigations (Courchesne et al., 2003; Muratori et al., 2012) and structural MRI studies (Courchesne et al., 2001; Redcay & Courchesne, 2005) observed that an increased brain size was typical of children, but not adults with ASD. Specifically, the increased cortical thickness in superior temporal and fusiform gyrus of the temporal lobe we observed is in line with findings of a recent investigation that analyze a subset of the ABIDE I cohort (Khundrakpam et al., 2017),

and could be related to the impairment of face processing, particularly in its dynamic aspects such as gaze, typical of subjects with ASD. In a similar vein, disruption in the lingual gyrus is involved in alterations of object/face recognition and following biological motion cues in ASD

(Ecker et al., 2015), since this region (along with lateral occipital cortex, fusiform gyrus and posterior superior temporal sulcus) is part of a network sustaining the aforementioned abilities. On the other hand, the IPL is thought to be part of the human Mirror Neuron System (MNS), the set of brain regions which are active both when participants perform an action and when they observe another person performing the same action (Rizzolatti & Craighero, 2004). The human MNS plays a key role in action understanding and imitation (Rizzolatti & Sinigaglia, 2010), and its disruption has been related to impairments in theory of mind and language in subjects with ASD (Gallese, 2007, 2008). Finally, we detected increased cortical thickness in the L inferior temporal region (ITG), which is consistent with increased gray matter volume in the same region observed by Cai et al. (Cai et al., 2018), in children with ASD. Since ITG is involved in language acquisition, its abnormal structure could be related to alterations in language development at least in the early stages of ASD.

Finally, consistent findings between the groups of adolescents and adults were detected, consisting in increased values in the population of subjects with ASD regarding: the volume of the L caudal anterior cingulate; the thickness SD of the L lingual gyrus; either the volume, the average and the SD of the thickness of the medial orbital frontal gyrus, bilaterally; either the volume and the average thickness of L transverse temporal gyrus. It is consistently reported that the developmental trajectory of cortical thickness in individuals with ASD deviates from the typical trajectory, even if studies do not agree with each other regarding the direction of the difference. For instance, the longitudinal study by Zielinski and colleagues (Zielinski et al., 2014), detected an overgrowth of the cortical thickness during early childhood, followed by an accelerated decline in mid-childhood, and a phase of *normalization* during adulthood. Other studies using an age-range similar to ours are in line with current findings, observing that the cerebral cortex thins less in ASD subjects compared to TD peers (Doyle-Thomas et al., 2013; Hardan, Muddasani et al., 2006; Sussman et al., 2015). As far as relevant findings in our cohort, the increased cortical thickness in the lingual gyrus of L hemisphere is consistent with a recent report on adults with ASD (Arunachalam Chandran et al., 2021), as well as with other studies showing a correlation between structural atypicalities in lingual gyrus of individuals with ASD and visual sensory abnormalities (Habata et al., 2021), or atypical social interaction (Turnbull et al., 2020). Moreover, two structures of the frontal regions seems to mostly differentiate adolescents and adults with ASD from TD peers: i) the medial orbitofrontal cortex is involved in the self-regulation of emotional states in relation to changes in social situations (Bachevalier & Loveland, 2006), and its volumetric alteration has been positively correlated with levels of circumscribed interests – a core feature of ASD (Hardan, Girgis, et al., 2006); ii) the caudal anterior cingulate is involved in processing the value of actions (Amodio & Frith, 2006), and its functional deficits have been linked to altered awareness of emotions and feelings of self and others in ASD (Zhou et al., 2016). The transverse temporal gyri -also known as Heschl's gyri-, are typically the location of the primary auditory cortex. Abnormal development of auditory cortex has been previously observed in children and adolescents with ASD (Prigge et al., 2013), and may constitute contribution to the core deficits in social communication of ASD subjects.

5. Conclusions

In conclusion, supported by the significant increase in the ASD vs. TD discrimination performance of ML classifiers in case the *NeuroHarmonize* preprocessing is implemented, we suggest its use in the analyses of multi-center MRI data. This is particularly relevant for studying disorders with very small effects on brain anatomy, which can be easily obscured by the confounding information due to the acquisition site.

CRediT authorship contribution statement

Sara Saponaro: Conceptualization, Methodology, Formal analysis, Software, Investigation, Visualization, Writing – original draft, Writing – review & editing. **Alessia Giuliano:** Conceptualization, Methodology, Data curation, Validation, Writing – original draft, Writing – review & editing. **Roberto Bellotti:** Validation, Writing – review & editing. **Angela Lombardi:** Conceptualization, Methodology, Formal analysis, Validation, Writing – original draft, Writing – review & editing. **Sabina Tangaro:** Conceptualization, Methodology, Validation, Writing – review & editing, Funding acquisition. **Piernicola Oliva:** Conceptualization, Methodology, Validation, Writing – review & editing, Funding acquisition. **Sara Calderoni:** Methodology, Validation, Writing – original draft, Writing – review & editing. **Alessandra Retico:** Conceptualization, Methodology, Formal analysis, Writing – original draft, Writing – review & editing, Validation, Supervision, Project administration, Funding acquisition.

Acknowledgments

This work has been partially supported by the INFN-CSN5 research project *Artificial Intelligence in Medicine (AIM)*, by the University of Sassari (Italy) (Fondo di Ateneo per la ricerca 2020) and by a grant from the IRCCS Fondazione Stella Maris (Ricerca Corrente, and the 5 1000 voluntary contributions, Italian Ministry of Health, n. 2768566). ALS position is funded by the Program Research for Innovation - REFIN funded by Regione Puglia (Italy) in the framework of the POR Puglia FESR FSE 2014-2020 Asse X - Azione 10.4, project code 928A7C98.

Appendix A. Supplementary data

Supplementary data to this article can be found online at <https://doi.org/10.1016/j.nicl.2022.103082>.

References

- Abraham, A., Milham, M.P., Martino, A.D., Craddock, R.C., Samaras, D., Thirion, B., Varo-quaux, G., 2017. Deriving reproducible biomarkers from multi-site resting-state data: An autism-based example. *NeuroImage* 147, 736–745. <https://doi.org/10.1016/j.neuroimage.2016.10.045>.
- American Psychiatric Association, A. et al. (2013). *Diagnostic and statistical manual of mental disorders* (5th ed.). American Psychiatric Association Washington, DC.
- Amodio, D., Frith, C., 2006. Amodio, d.m. frith, c.d. meeting of minds: The medial frontal cortex and social cognition. *nat. rev. neurosci.* 7, 268–277. *Nat. Rev. Neurosci.* 7, 268–277. <https://doi.org/10.1038/nrn1884>.
- Arbabshirani, M.R., Plis, S., Sui, J., Calhoun, V.D., 2017. Single subject prediction of brain disorders in neuroimaging: Promises and pitfalls. *NeuroImage* 145, 137–165.
- Arunachalam Chandran, V., Pliatsikas, C., Neufeld, J., O'Connell, G., Haffey, A., DeLuca, V., Chakrabarti, B., 2021. Brain structural correlates of autistic traits across the diagnostic divide: A grey matter and white matter microstructure study. *NeuroImage: Clinical* 32, 102897. <https://doi.org/10.1016/j.nicl.2021.102897>.
- Avanzo, M., Porzio, M., Lorenzon, L., Milan, L., Sghedoni, R., Russo, G., Massafra, R., Fanizzi, A., Barucci, A., Ardu, V., Branchini, M., Giannelli, M., Gallio, E., Cilla, S., Tangaro, S., Lombardi, A., Pirrone, G., De Martin, E., Giuliano, A., Belmonte, G., Russo, S., Rampado, O., Mettivier, G., 2021. Artificial intelligence applications in medical imaging: A review of the medical physics research in Italy. *Physica Med.* 83, 221–241.
- Bachevalier, J., Loveland, K., 2006. The orbitofrontal-amygdala circuit and self-regulation of social-emotional behavior in autism. *Neurosci. Biobehav. Rev.* 30, 97–117. <https://doi.org/10.1016/j.neubiorev.2005.07.002>.
- Bhaumik, R., Pradhan, A., Das, S., Bhaumik, D.K., 2018. Predicting Autism Spectrum Disorder Using Domain-Adaptive Cross-Site Evaluation. *Neuroinform* 16 (2), 197–205.
- Breiman, L., 2001. *Random forests*.
- Monte-Rubio, C.G., Segura, B., Strafella, P.A., van Eimeren, T., Ibarretxe-Bilbao, N., Diez-Cirarda, M., Eggers, C., Lucas-Jiménez, O., Ojeda, N., Peña, J., Ruppert, M.C., Sala-Llonch, R., Theis, H., Uribe, C., Junque, C., 2022. Parameters from site classification to harmonize mri clinical studies: Application to a multi-site parkinson's disease dataset. *Hum. Brain Mapp.* 1–13. <https://doi.org/10.1002/hbm.25838>.
- Cai, J., Hui, X., Guo, K., Yang, P., Situ, M., Huang, Y., 2018. Increased left inferior temporal gyrus was found in both low function autism and high function autism. *Front. Psychiatry* 9. <https://doi.org/10.3389/fpsyh.2018.00542>.
- Calderoni, S., Retico, A., Biagi, L., Tancredi, R., Muratori, F., Tosetti, M., 2012. Female children with autism spectrum disorder: An insight from mass-univariate and pattern classification analyses. *NeuroImage* 59 (2), 1013–1022.

- Chen, X., Ishwaran, H., 2012. Random forests for genomic data analysis. *Genomics* 99 (6), 323–329. <https://doi.org/10.1016/j.ygeno.2012.04.003>.
- Cohen, J., 1988. *Statistical power analysis for the behavioral sciences*, (2nd ed.). Routledge.
- Courchesne, E., Karns, C.M., Davis, H.R., Ziccardi, R., Carper, R.A., Tigue, Z.D., Chisum, H.J., Moses, P., Pierce, K., Lord, C., Lincoln, A.J., Pizzo, S., Schreibman, L., Haas, R.H., Akshoomoff, N.A., Courchesne, R.Y., 2001. Unusual brain growth patterns in early life in patients with autistic disorder: An MRI study. *Neurology* 57 (2), 245–254.
- Deshpande, G., Liberio, L.E., Sreenivasan, K.R., Deshpande, H.D., Kana, R.K., 2013. Identification of neural connectivity signatures of autism using machine learning. *Front. Hum. Neurosci.* 7 <https://doi.org/10.3389/fnhum.2013.00670>.
- Di Martino, A., Yan, C.-G., Li, Q., Denio, E., Castellanos, F.X., Alaerts, K., Anderson, J.S., Assaf, M., Bookheimer, S.Y., Dapretto, M., Deen, B., Delmonte, S., Dinstein, I., Ertl-Wagner, B., Fair, D.A., Gallagher, L., Kennedy, D.P., Keown, C.L., Keysers, C., Lainhart, J.E., Lord, C., Luna, B., Menon, V., Minshew, N.J., Monk, C.S., Mueller, S., Müller, R.-A., Nebel, M.B., Nigg, J.T., O’Hearn, K., Pelphrey, K.A., Peltier, S.J., Rudie, J.D., Sunaert, S., Thio, M., Tyszka, J.M., Uddin, L.Q., Verhoeven, J.S., Wenderoth, N., Wiggins, J.L., Mostofsky, S.H., Milham, M.P., 2014. The autism brain imaging data exchange: Towards a large-scale evaluation of the intrinsic brain architecture in autism. *Mol. Psychiatry* 19 (6), 659–667.
- Di Martino, A., O’Connor, D., Chen, B., Alaerts, K., Anderson, J.S., Assaf, M., Balsters, J. H., Baxter, L., Beggiani, A., Bernaerts, S., Blanken, L.M.E., Bookheimer, S.Y., Braden, B.B., Byrge, L., Castellanos, F.X., Dapretto, M., Delorme, R., Fair, D.A., Fishman, I., Fitzgerald, J., Gallagher, L., Keehn, R.J.J., Kennedy, D.P., Lainhart, J.E., Luna, B., Mostofsky, S.H., Müller, R.-A., Nebel, M.B., Nigg, J.T., O’Hearn, K., Solomon, M., Toro, R., Vaidya, C.J., Wenderoth, N., White, T., Craddock, R.C., Lord, C., Leventhal, B., Milham, M.P., 2017. Enhancing studies of the connectome in autism using the autism brain imaging data exchange ii. *Sci. Data* 4 (1), 170010. <https://doi.org/10.1038/sdata.2017.10>.
- Doyle-Thomas, K., Duerden, E., Taylor, M., Lerch, J., Soorya, L., Wang, A.T., Fan, J., Hollander, E., Anagnostou, E., 2013. Effects of age and symptomatology on cortical thickness in autism spectrum disorders. *Res. Autism Spectrum Disorders* 7, 141–150. <https://doi.org/10.1016/j.rasd.2012.08.004>.
- Ecker, C., Marquand, A., Mourao-Miranda, J., Johnston, P., Daly, E.M., Brammer, M.J., Maltezos, S., Murphy, C.M., Robertson, D., Williams, S.C., Murphy, D.G.M., 2010a. Describing the Brain in Autism in Five Dimensions-Magnetic Resonance Imaging-Assisted Diagnosis of Autism Spectrum Disorder Using a Multiparameter Classification Approach. *J. Neurosci.* 30 (32), 10612–10623. <https://doi.org/10.1523/JNEUROSCI.5413-09.2010>.
- Ecker, C., Bookheimer, S.Y., Murphy, D.G., 2015. Neuroimaging in autism spectrum disorder: Brain structure and function across the lifespan. *Lancet Neurol.* 14 (11), 1121–1134. [https://doi.org/10.1016/S1474-4422\(15\)00050-2](https://doi.org/10.1016/S1474-4422(15)00050-2).
- Ecker, C., Rocha-Rego, V., Johnston, P., Mourao-Miranda, J., Marquand, A., Daly, E.M., Brammer, M.J., Murphy, C., Murphy, D.G., 2010b. Investigating the predictive value of whole-brain structural MR scans in autism: A pattern classification approach. *NeuroImage* 49 (1), 44–56.
- Ferrari, E., Bosco, P., Calderoni, S., Oliva, P., Palumbo, L., Spera, G., Fantacci, M. E., & Retico, A. (2020). Dealing with confounders and outliers in classification medical studies: The autism spectrum disorders case study. *Artif. Intell. Med.*, 108. <https://doi.org/10.1016/j.artmed.2020.101926>.
- Ferrari, E., Retico, A., Bacciu, D., 2020b. Measuring the effects of confounders in medical super-vised classification problems: The confounding index (ci). *Artif. Intell. Med.* 103, 101804. <https://doi.org/10.1016/j.artmed.2020.101804>.
- Fischl, B., 2012. *FreeSurfer*. *FreeSurfer* 62 (2), 774–781.
- Fortin, J.P., Cullen, N., Sheline, Y.L., Taylor, W.D., Aselcioglu, I., Cook, P.A., Adams, P., Cooper, C., Fava, M., McGrath, P.J., McInnis, M., Phillips, M.L., Trivedi, M.H., Weissman, M.M., Shinohara, R.T., 2018. Harmonization of cortical thickness measurements across scanners and sites. *NeuroImage* 167, 104–120. <https://doi.org/10.1016/j.neuroimage.2017.11.024>.
- Fortin, J.P., Parker, D., Tunç, B., Watanabe, T., Elliott, M.A., Ruparel, K., Roalf, D.R., Satterthwaite, T.D., Gur, R.C., Gur, R.E., Schultz, R.T., Verma, R., Shinohara, R.T., 2017. Harmonization of multi-site diffusion tensor imaging data. *NeuroImage* 161, 149–170. <https://doi.org/10.1016/j.neuroimage.2017.08.047>.
- Gallese, V., 2007. Before and below ‘theory of mind’: Embodied simulation and the neural correlates of social cognition. *Philos. Trans. R. Soc. London Series B, Biol. Sci.* 362, 659–669. <https://doi.org/10.1098/rstb.2006.2002>.
- Gallese, V., 2008. Mirror neurons and the social nature of language: The neural exploitation hypothesis. *Soc. Neurosci.* 3 (3–4), 317–333.
- Gao, J., Chen, M., Li, Y., Gao, Y., Li, Y., Cai, S., Wang, J., 2021. Multisite autism spectrum disorder classification using convolutional neural network classifier and individual morphological brain networks. *Front. Neurosci.* 14, 1–10. <https://doi.org/10.3389/fnins.2020.629630>.
- Georgiades, S., Szatmari, P., Boyle, M., Hanna, S., Duku, E., Zwaigenbaum, L., Bryson, S., Fombonne, E., Volden, J., Miranda, P., Smith, I., Roberts, W., Vaillancourt, T., Waddell, C., Bennett, T., Thompson, A., & in ASD Study Team, P. (2013). Investigating phenotypic heterogeneity in children with autism spectrum disorder: A factor mixture modeling approach. *J. Child Psychol. Psychiatry*, 54 (2), 206–215. <https://doi.org/https://doi.org/10.1111/j.1469-7610.2012.02588.x>.
- Gori, I., Giuliano, A., Muratori, F., Saviozzi, I., Oliva, P., Tancredi, R., Cosenza, A., Tosetti, M., Calderoni, S., Retico, A., 2015. Gray Matter Alterations in Young Children with Autism Spectrum Disorders: Comparing Morphometry at the Voxel and Regional Level. *J. Neuroimaging* 25 (6), 866–874.
- Guan, H., Liu, Y., Yang, E., Yap, P.T., Shen, D., Liu, M., 2021. Multi-site mri harmonization via attention-guided deep domain adaptation for brain disorder identification. *Med. Image Anal.* 71, 102076. <https://doi.org/10.1016/j.media.2021.102076>.
- Haar, S., Berman, S., Behrmann, M., Dinstein, I., 2016. Anatomical abnormalities in autism? *Cereb. Cortex* 26 (4), 1440–1452.
- Habata, K., Cheong, Y., Kamiya, T., Shiotsu, D., Omori, I.M., Okazawa, H., Jung, M., Kosaka, H., 2021. Relationship between sensory characteristics and cortical thickness/volume in autism spectrum disorders. *Transl. Psychiatry* 11 (1), 1–7.
- Hanley, J.A., McNeil, B.J., 1982. The meaning and use of the area under a receiver operating characteristic (roc) curve. *Radiology* 143 (1), 29–36.
- Hardan, A., Giris, R., Lacerda, A., Yorbik, O., Kilpatrick, M., Keshavan, M., Minshew, N., 2006a. Magnetic resonance imaging study of the orbitofrontal cortex in autism. *J. Child Neurol.* 21, 866–871. <https://doi.org/10.1177/08830738060210100701>.
- Hardan, A., Muddasani, S., Vemulapalli, M., Keshavan, M., Minshew, N., 2006b. An mri study of increased cortical thickness in autism. *Am. J. Psychiatry* 163, 1290–1292. <https://doi.org/10.1176/appi.ajp.163.7.1290>.
- Hastie, T., Tibshirani, R., 1986. Generalized Additive Models. *Stat. Sci.* 1 (3), 297–310. <https://doi.org/10.1214/ss/1177013604>.
- Heinsfeld, A.S., Franco, A.R., Craddock, R.C., Buchweitz, A., Meneguzzi, F., 2018. Identification of autism spectrum disorder using deep learning and the abide dataset. *NeuroImage: Clinical* 17, 16–23. <https://doi.org/10.1016/j.nicl.2017.08.017>.
- Ingalhalikar, M., Parker, D., Bloy, L., Roberts, T.P., Verma, R., 2011. Diffusion based abnormality markers of pathology: Toward learned diagnostic prediction of ASD. *NeuroImage* 57 (3), 918–927. <https://doi.org/10.1016/j.neuroimage.2011.05.023>.
- Ingalhalikar, M., Shinde, S., Karmarkar, A., Rajan, A., Rangaprakash, D., Deshpande, G., 2021. Functional Connectivity-Based Prediction of Autism on Site Harmonized ABIDE Dataset. *IEEE Trans. Biomed. Eng.* 68 (12), 3628–3637.
- Jiao, Y., Chen, R., Ke, X., Chu, K., Lu, Z., Herskovits, E.H., 2010. Predictive models of autism spectrum disorder based on brain regional cortical thickness. *NeuroImage* 50 (2), 589–599. <https://doi.org/10.1016/j.neuroimage.2009.12.047>.
- Johnson, W.E., Li, C., Rabinovic, A., 2007. Adjusting batch effects in microarray expression data using empirical Bayes methods. *Biostatistics* 8 (1), 118–127. <https://doi.org/10.1093/biostatistics/kxj037>.
- Jung, M., Tu, Y., Lang, C. A., Ortiz, A., Park, J., Jorgenson, K., Kong, X.-J., & Kong, J. (2019). Decreased structural connectivity and resting-state brain activity in the lateral occipital cortex is associated with social communication deficits in boys with autism spectrum disorder [Mapping diseased brains]. *NeuroImage*, 190, 205–212. <https://doi.org/https://doi.org/10.1016/j.neuroimage.2017.09.031>.
- Katuwal, G.J., Baum, S.A., Cahill, N.D., Michael, A.M., 2016. Divide and conquer: Subgrouping of asd improves asd detection based on brain morphometry. *PLoS ONE* 11 (4), 1–24. <https://doi.org/10.1371/journal.pone.0153331>.
- Khundrakam, B., Lewis, J., Kostopoulos, P., Carbonell, F., Evans, A., 2017. Cortical thickness abnormalities in autism spectrum disorders through late childhood, adolescence, and adulthood: A large-scale mri study. *Cereb. Cortex* 27, 1–11. <https://doi.org/10.1093/cercor/bhx038>.
- Klein, A., Tourville, J., 2012. 101 labeled brain images and a consistent human cortical labeling protocol. *Front. Neurosci.* <https://doi.org/10.3389/fnins.2012.00171>.
- Kraemer, H.C., Yesavage, J.A., Taylor, J.L., Kupfer, D., 2000. How can we learn about developmental processes from cross-sectional studies, or can we? *Am. J. Psychiatry* 157 (12), 163–171. <https://doi.org/10.1176/appi.ajp.157.2.163>.
- Lai, M.C., Lombardo, M.V., Suckling, J., Ruigrok, A.N., Chakrabarti, B., Ecker, C., Deoni, S.C., Craig, M.C., Murphy, D.G., Bullmore, E.T., Baron-Cohen, S., 2013. Biological sex affects the neurobiology of autism. *Brain* 136, 2799–2815. <https://doi.org/10.1093/brain/awt216>.
- Lai, M.-C., Kasse, C., Besney, R., Bonato, S., Hull, L., Mandy, W., Szatmari, P., Ameis, S. H., 2019. Prevalence of co-occurring mental health diagnoses in the autism population: a systematic review and meta-analysis. *Lancet Psychiatry* 6 (10), 819–829.
- Li, D., Karnath, H.-O., Xu, X., 2017. Candidate Biomarkers in Children with Autism Spectrum Disorder: A Review of MRI Studies. *Neurosci. Bull.* 33 (2), 219–237.
- Linn, K.A., Gaonkar, B., Satterthwaite, T.D., Doshi, J., Davatzikos, C., Shinohara, R.T., 2016. Control-group feature normalization for multivariate pattern analysis of structural MRI data using the support vector machine. *NeuroImage* 132, 157–166.
- Lombardi, A., Amoroso, N., Diacono, D., Monaco, A., Tangaro, S., Bellotti, R., 2020. Extensive evaluation of morphological statistical harmonization for brain age prediction. *Brain Sci.* 10 (6), 364.
- Metz, C.E., 2006. Receiver operating characteristic analysis: A tool for the quantitative evaluation of observer performance and imaging systems. *J. Am. College Radiol.* 3, 413–422. <https://doi.org/10.1016/j.jacr.2006.02.021>.
- Muratori, F., Calderoni, S., Apicella, F., Filippi, T., Santocchi, E., Calugi, S., Cosenza, A., Tancredi, R., Narzisi, A., 2012. Tracing back to the onset of abnormal head circumference growth in Italian children with autism spectrum disorder. *Res. Autism Spectrum Disorders* 6, 442–449. <https://doi.org/10.1016/j.rasd.2011.07.004>.
- Nielsen, J., Zielinski, B.A., Fletcher, P.T., Alexander, A.L., Lange, N.T., Bigler, E.D., Lainhart, J.E., Anderson, J.S., 2013. Multisite functional connectivity mri classification of autism: Abide results. *Front. Hum. Neurosci.* 7.
- Ojala, M., Garriga, G.C., 2009. Permutation tests for studying classifier performance. *Ninth IEEE International Conference on Data Mining 2009*, 908–913. <https://doi.org/10.1109/ICDM.2009.108>.
- Pagnozzi, A.M., Conti, E., Calderoni, S., Fripp, J., Rose, S.E., 2018. A systematic review of structural mri biomarkers in autism spectrum disorder: A machine learning perspective. *Int. J. Dev. Neurosci.* 71 (1), 68–82. <https://doi.org/10.1016/j.ijdevneu.2018.08.010>.
- Pedregosa, F., Varoquaux, G., Gramfort, A., Michel, V., Thirion, B., Grisel, O., Blondel, M., Prettenhofer, P., Weiss, R., Dubourg, V., Vanderplas, J., Passos, A.,

- Cournapeau, D., Brucher, M., Perrot, M., Duchesnay, E., 2011. Scikit-learn: Machine learning in Python. *J. Mach. Learn. Res.* 12, 2825–2830.
- Pomponio, R., Erus, G., Habes, M., Doshi, J., Srinivasan, D., Mamourian, E., Bashyam, V., Nasrallah, I.M., Satterthwaite, T.D., Fan, Y., Launer, L.J., Masters, C.L., Maruff, P., Zhuo, C., Völzke, H., Johnson, S.C., Fripp, J., Koutsouleris, N., Wolf, D.H., Gur, R., Gur, R., Morris, J., Albert, M.S., Grabe, H.J., Resnick, S.M., Bryan, R.N., Wolk, D.A., Shinohara, R.T., Shou, H., Davatzikos, C., 2020. Harmonization of large mri datasets for the analysis of brain imaging patterns throughout the lifespan. *NeuroImage* 208, 116450.
- Prigge, M.D., Bigler, E.D., Fletcher, P.T., Zielinski, B.A., Ravichandran, C., Anderson, J., Froehlich, A., Abildskov, T., Papadopolous, E., Maasberg, K., Nielsen, J.A., Alexander, A.L., Lange, N., Lainhart, J., 2013. Longitudinal heschl's gyrus growth during childhood and adolescence in typical development and autism. *Autism Res.* 6 (2), 78–90.
- Qin, K., Lei, D., Pinaya, W. H., Pan, N., Li, W., Zhu, Z., Sweeney, J. A., Mechelli, A., & Gong, Q. (2022). Using graph convolutional network to characterize individuals with major depressive disorder across multiple imaging sites. *eBioMedicine*, 78, 103977. <https://doi.org/https://doi.org/10.1016/j.ebiom.2022.103977>.
- Redcay, E., Courchesne, E., 2005. When is the brain enlarged in autism? a meta-analysis of all brain size reports. *Biol. Psychiatry* 58, 1–9. <https://doi.org/10.1016/j.biopsych.2005.03.026>.
- Reticco, A., Giuliano, A., Tancredi, R., Cosenza, A., Apicella, F., Narzisi, A., Biagi, L., Tosetti, M., Muratori, F., Calderoni, S., 2016. The effect of gender on the neuroanatomy of children with autism spectrum disorders: A support vector machine case-control study. *Molecular Autism* 7. <https://doi.org/10.1186/s13229-015-0067-3>.
- Rizzolatti, G., Craighero, L., 2004. The mirror-neuron system. *Annu. Rev. Neurosci.* 27, 169–192. <https://doi.org/10.1146/annurev.neuro.27.070203.144230>.
- Rizzolatti, G., Sinigaglia, C., 2010. The functional role of the parieto-frontal mirror circuit: Interpretations and misinterpretations. *Nat. Rev. Neurosci.* 11, 264–274. <https://doi.org/10.1038/nrn2805>.
- Sullivan, P., Daly, M., O'Donovan, M., 2012. Disease mechanisms genetic architectures of psychiatric disorders: The emerging picture and its implications. *Nat. Rev. Genet.* 13, 537–551. <https://doi.org/10.1038/nrg3240>.
- Sussman, D., Leung, R.C., Vogan, V.M., Lee, W., Trelle, S., Lin, S., Cassel, D.B., Chakravarty, M.M., Lerch, J.P., Anagnostou, E., Taylor, M.J., 2015. The autism puzzle: Diffuse but not pervasive neuroanatomical abnormalities in children with ASD. *NeuroImage: Clinical* 8, 170–179.
- Turnbull, A., Garfinkel, S., Ho, N., Critchley, H., Bernhardt, B., Jefferies, E., Smallwood, J., 2020. Word up - experiential and neurocognitive evidence for associations between autistic symptomology and a preference for thinking in the form of words. *Cortex* 128. <https://doi.org/10.1016/j.cortex.2020.02.019>.
- Uddin, L.Q., Supekar, K., Lynch, C.J., Khouzam, A., Phillips, J., Feinstein, C., Ryali, S., & Menon, V. (2013). Salience Network–Based Classification and Prediction of Symptom Severity in Children With Autism. *JAMA Psychiatry*, 70 (8), 869. <https://doi.org/10.1001/jamapsychiatry.2013.104>.
- Vargason, T., Grivas, G., Hollowood-Jones, K.L., Hahn, J., 2020. Towards a Multivariate Biomarker-Based Diagnosis of Autism Spectrum Disorder: Review and Discussion of Recent Advancements. *Seminars Pediatric Neurol.* 34, 100803 <https://doi.org/10.1016/j.spen.2020.100803>.
- Wang, R., Chaudhari, P., Davatzikos, C., 2022. Embracing the disharmony in medical imaging: A simple and effective framework for domain adaptation. *Med. Image Anal.* 76, 102309 <https://doi.org/10.1016/j.media.2021.102309>.
- Wolfers, T., Floris, D.L., Dinga, R., van Rooij, D., Isakoglou, C., Kia, S.M., Zabihi, M., Llera, A., Chowdanayaka, R., Kumar, V.J., Peng, H., Laidi, C., Batalle, D., Dimitrova, R., Charman, T., Loth, E., Lai, M.-C., Jones, E., Baumeister, S., Moessnang, C., Banaschewski, T., Ecker, C., Dumas, G., O'Muircheartaigh, J., Murphy, D., Buitelaar, J.K., Marquand, A.F., Beckmann, C.F., 2019. From pattern classification to stratification: towards conceptualizing the heterogeneity of Autism Spectrum Disorder. *Neurosci. Biobehav. Rev.* 104, 240–254.
- Wood, S. N. (2017). Generalized additive models: An introduction with r, second edition.
- Wrobel, J., Martin, M.L., Bakshi, R., Calabresi, P.A., Elliot, M., Roalf, D., Gur, R.C., Gur, R.E., Henry, R.G., Nair, G., Oh, J., Papinutto, N., Pelletier, D., Reich, D.S., Rooney, W.D., Satterthwaite, T.D., Stern, W., Prabhakaran, K., Sicotte, N.L., Shinohara, R.T., Goldsmith, J., 2020. Intensity warping for multisite mri harmonization. *NeuroImage* 223, 117242.
- Zhou, Y., Shi, L., Cui, X., Wang, S., & Luo, X. (2016). Functional connectivity of the caudal anterior cingulate cortex is decreased in autism. *PLoS one*, 11, e0151879. <https://doi.org/10.1371/journal.pone.0151879>.
- Zielinski, B., Prigge, M., Nielsen, J., Froehlich, A., Abildskov, T., Anderson, J., Fletcher, P., Campbell, K., Travers, B., Lange, N., Alexander, A., Bigler, E., & Lainhart, J. (2014). Longitudinal changes in cortical thickness in autism and typical development. *Brain: J. Neurol.*, 137. <https://doi.org/10.1093/brain/awu083>.